Hindawi
Mathematical Problems in Engineering
Volume 2020, Article ID 5319408, 15 pages
https://doi.org/10.1155/2020/5319408

Research Article

A Two-Stage Scheduling RPC Based on Time-Varying Coefficient Information of State-Dependent ARX Model

Feng Zhou,[1] **Peidong Zhu**,[1] **Minghua Xie**,[1] **Jun Wu**,[2] **and Lihua Cao**[1]

[1]*School of Electronic Information and Electrical Engineering, Changsha University, Changsha, Hunan 410022, China*
[2]*School of Electrical and Information Engineering, Changsha University of Science and Technology, Changsha, Hunan 410076, China*

Correspondence should be addressed to Peidong Zhu; zpd136@sina.com

Received 4 September 2019; Accepted 23 January 2020; Published 7 March 2020

Academic Editor: Carlos-Renato Vázquez

A two-stage scheduling robust predictive control (RPC) algorithm, which is based on the time-varying coefficient information of the state-dependent ARX (SD-ARX) model, is designed for the output tracking control of a class of nonlinear systems. First, by using the parameter variation range information of the SD-ARX, a strategy for constructing the system's polytopic model is designed. To further reduce the conservativeness of the convex polytopic sets which are designed to wrap the system's future dynamics, the variation range information of the SD-ARX model's parameters is also considered and compressed. In this method, the polytopic state-space model of the system is constructed directly based on the special structure of the SD-ARX model itself, and there is no need to make such assumption that the bounds on the parameter's variation range in the system model are known or measurable. And then, a two-stage scheduling RPC algorithm is designed for the output tracking control. A numerical example is presented to demonstrate the effectiveness of the proposed RPC strategy.

1. Introduction

Model predictive control (MPC), which directly uses the mathematical model to predict the future behavior of the system, has been widely studied in the past decade [1]. Considering that the actual systems are always nonlinear and the working conditions often undergo uncertainties, which may have significant impact on the system [2], how to deal with the system uncertainties, whether in the form of external disturbance or parameter estimation error, is still the key issue that needs to be solved in the MPCs [3]. Considering that models with polytopic description can be effectively used to include the uncertainties of the nonlinear systems, the MPC strategies based on these types of models have been widely studied. For the polytopic LPV model, Kothare et al. [4] proposed an RPC algorithm and used the linear matrix inequalities (LMIs) to settle the control gains in the robust controller. Based on the min-max principle, Lu and Arkun [5, 6] designed a state feedback predictive control strategy for an uncertain LPV system without external disturbance. Mayne et al. [7] proposed an RPC strategy for linear systems with external bounded disturbances. He et al. [8] designed an RPC algorithm for constrained continuous-time nonlinear systems with bounded disturbances. A neural network model-based RPC strategy considering the uncertain but bounded disturbances is proposed for constrained discrete-time nonlinear systems [9]. For constrained nonlinear systems, He et al. [10] designed a quasi-min-max RPC algorithm. Although many achievements have been achieved in the research of RPC algorithms for systems with polytopic description [4–10], they mainly focused on the state adjustment or output tracking problems based on certain restrictive assumptions; for example, the steady-state information of the system is accurately known or measured [11]. In these methods, to derive the system's LPV model, the polynomial model of the system usually needs to be linearized at the operating point of the system, and the obtained LPV model

may be different when the operating point changed [11]. Considering that there also exist many systems in practice with unmeasured steady-state knowledge due to uncertainty or disturbance [11, 12], it is meaningful to develop new RPC strategies which can overcome the above difficulties [13].

Some researchers have paid their attention to the output feedback RPCs based on the state estimators. For discrete-time systems with bounded disturbances, Mayne et al. [14] proposed an output feedback controller design method. Based on the min-max principle, Park et al. [12] proposed a robust output feedback MPC scheme for the LPV systems. Ding [15] designed an output feedback RPC for the LPV system with external disturbance. Ding et al. [16] also designed an output feedback RPC for the LPV models with norm-bounded disturbances. Based on a high-gain observer, Du et al. [17] studied a robust output feedback MPC for dynamically positioned ships with uncertain parameters. However, considering that the state estimation errors exist in the state estimators [12–15], the synthesis procedures of the output feedback RPCs may be more complicated than the state feedback MPCs [4–8]. Moreover, to ensure the system's variable constraints, the synthesis process of the output feedback RPCs may be further complicated [11, 18]. In general, the complex nonlinear systems are more accessible to be modeled as the input-output formal equations. So, the RPC strategies directly based on the system's input-output model are valuable [18, 19]. Directly based on the system's input-output model, Ding and Zou [18] designed an output feedback RPC synthesis approach. Abbas et al. [19] proposed an RPC strategy for the system described by the LPV model in input-output form. In this paper, an RPC strategy directly based on the data-driven state-dependent (SD) autoregressive (SD-ARX) model with exogenous variable is studied. It distinguishes from the RPC strategies under the assumption that the state of the system is measurable [4–8] or can be obtained by the state estimator [12–15], and the steady-state information is never used in the designing process of the robust predictive controller.

The SD-ARX model is a quasi-LPV model with functional coefficients and is often used in nonlinear system modeling [20]. Using RBF to approximate the state-dependent coefficients of the SD-ARX model generates the RBF-ARX model [21, 22]. These type model-based MPC strategies have been successfully applied to many systems, such as the industrial drying process [23, 24], the NOx decomposition process [21, 25], the water tank system [26], and the ship's tracking control [27]. But, most of these literatures [21–26] are limited to nominal conditions, and the stabilities of these MPCs are also difficult to guarantee. Based on the RBF-ARX model, Peng et al. [28] designed a min-max MPC algorithm for nonlinear systems without external disturbance. Zhou et al. [29] proposed a one-stage scheduling quasi-min-max MPC algorithm, in which the external bounded disturbance is considered. What is more, Zhou et al. [30] further studied a two-stage scheduling quasi-min-max MPC algorithm based on the RBF-ARX model. Although some results have been achieved, the current literatures [28–30] are mainly focused on using the parameter bound information of the SD-ARX model to wrap the system's future dynamics, and these types of methods have serious conservatism when constructing the system's state-space model. To reduce the conservativeness of these type of methods, the variation range information of the SD-ARX model's parameters is further considered in this paper to compress the size of the convex polytopic sets which are designed to wrap the system's future dynamics. And then, the control performance of the subsequent RPC algorithm may be improved. Moreover, it is no need to make such assumption that the bounds on the parameter's variation range in the LPV model are available [31–34]. The polytopic state-space model of the system is constructed directly based on the special structure of the SD-ARX model itself.

The rest of the paper is as follows: by using the SD-ARX model's parameter variation range information, the construction process of the system's polytopic LPV state-space model is introduced in Section 2. And then, a two-stage scheduling robust predictive control (RPC) algorithm based on the constructed LPV state-space model is designed in Section 3. An example is presented to illustrate the design procedure in Section 4. The conclusions are drawn in Section 5.

2. Construction of the System's Polytopic State-Space Model

The class of nonlinear systems, which can be depicted with the following autoregressive model [21], is considered:

$$y(t+1) = f\left(y(t), \ldots, y\left(t-k_\alpha+1\right), u\left(t-k_d\right), \ldots, u\left(t-k_\beta-k_d+1\right)\right) + \varsigma(t+1), \tag{1}$$

where $y(t) \in \mathfrak{R}$ and $u(t) \in \mathfrak{R}$ are the system's output and input; $\varsigma(t+1) \in \mathfrak{R}$ is the white noise interference term; and k_α and k_β are the variable orders, and k_d is the variable time delay. If the nonlinear mapping $f(\cdot)$ is continuously differentiable at any working state, model (1) can be represented by the following SD-ARX model [21]:

$$y(t+1)=\varphi_0(s(t))+\sum_{i=0}^{k_\alpha-1}\varphi_{\alpha,i}(s(t))y(t-i)+\sum_{i=k_d}^{k_\beta+k_d-1}\varphi_{\beta,i}(s(t))u(t-i)+\varsigma(t+1),$$

$$\begin{cases}\varphi_0(s(t))=\kappa_0^0+\sum_{h=1}^{m}\kappa_h^0 e^{\left\{-\sigma_h^\alpha\left\|s(t)-\nu_h^\alpha\right\|_2^2\right\}},\\ \varphi_{j,i}(s(t))=\kappa_{i,0}^j+\sum_{h=1}^{m}\kappa_{i,h}^j e^{\left\{-\sigma_h^j\left\|s(t)-\nu_h^j\right\|_2^2\right\}},\\ \nu_h^j=\left[\nu_{h,1}^j,\nu_{h,2}^j,\ldots,\nu_{h,d}^j\right]^{\mathrm{T}},\\ j=\alpha,\beta,\end{cases}\tag{2}$$

where m and d are the model orders; $s(t)=[s_{t,1},s_{t,2},\ldots,s_{t,d}]^{\mathrm{T}}$ is called the state vector, and it may include delayed inputs or outputs, or other signals that can be measured; $\varphi_0(s(t))$, $\varphi_{\alpha,i}(s(t))$, and $\varphi_{\beta,i}(s(t))$ are the state-dependent functional coefficients; σ_h^j and ν_h^j are the widths and centers of the neural network, respectively; κ_0^0, κ_h^0, $\kappa_{i,0}^j$, and $\kappa_{i,h}^j$ are the linear weights of the neural network; and $\|\cdot\|_2$ represents the vector 2-norm. The nonlinear parameters $\theta_N=\left\{\sigma_h^j,\nu_h^j\right\}$ and linear parameters $\theta_L=\left\{\kappa_0^0,\kappa_h^0,\kappa_{i,0}^j,\kappa_{i,h}^j\right\}$ in model (2) are optimized by the regularized SNPOM [22]. The details of the regularized SNPOM algorithm can be found in Ref. [22], which is omitted here.

To obtain a more general system model, first, the term representing the bounded unknown disturbance is added into the SD-ARX model (2), thus obtaining

$$\begin{aligned}y(t+1)=&\varphi_0(s(t))+\sum_{i=0}^{k_\alpha-1}\varphi_{\alpha,i}(s(t))y(t-i)\\&+\sum_{i=k_d}^{k_\beta+k_d-1}\varphi_{\beta,i}(s(t))u(t-i)+\zeta(t+1),\end{aligned}\tag{3}$$

where $\delta>0$ is a constant and $\{|\zeta(t+1)|\le\delta\}$ represents the bounded unknown disturbance including the modeling error. And then, model (3) can be rewritten as follows:

$$y(t+1)=\varphi_{0,t}+\sum_{i=0}^{k_n-1}\alpha_{i+1,t}y(t-i)+\sum_{i=0}^{k_n-1}\beta_{i+1,t}u(t-i)+\zeta(t+1),$$

$$\begin{cases}\varphi_{0,t}=\varphi_0(s(t)),\\ \alpha_{i+1,t}=\begin{cases}\kappa_{i,0}^\alpha+\sum_{h=1}^{m}\kappa_{i,h}^\alpha e^{\left\{-\sigma_h^\alpha\left\|s(t)-\nu_h^\alpha\right\|_2^2\right\}}, & (0\le i\le k_\alpha-1),\\ 0, & \text{else},\end{cases}\\ \beta_{i+1,t}=\begin{cases}\kappa_{i,0}^\beta+\sum_{h=1}^{m}\kappa_{i,h}^\beta e^{\left\{-\sigma_h^\beta\left\|s(t)-\nu_h^\beta\right\|_2^2\right\}}, & \left(k_d\le i\le k_\beta+k_d-1\right),\\ 0, & \text{else},\end{cases}\\ k_n=\max\left(k_\alpha,k_\beta+k_d\right),\quad |\zeta(t+1)|\le\delta.\end{cases}\tag{4}$$

Next, define the system deviation inputs and outputs as

$$\begin{cases}\overline{u}(t+j_1)=u(t+j_1)-u(t+j_1-1), & j_1=0,-1,-2,\ldots,\\ \overline{y}(t+j_2)=y(t+j_2)-y_{r,t+j_2}, & j_2=1,-1,-2,\ldots,\\ y_{r,t+1}=\eta y(t)+(1-\eta)y_r, & 0\le\eta<1,\\ y_{r,t+j_2}=y_r, & j_2<1,\end{cases}\tag{5}$$

where y_r is the expected output and the expected output sequence $y_{r,t+j_2}$ is designed to be an exponential decay curve. Based on models (4) and (5), the output deviation of the one-step-forward prediction $\overline{y}(t+1\,|\,t)$ of the model (4) is derived as follows:

$$\overline{y}(t+1\,|\,t)=\sum_{i=0}^{k_n-1}\alpha_{i+1,t}\overline{y}(t-i)+\sum_{i=0}^{k_n-1}\beta_{i+1,t}\overline{u}(t-i)+\vartheta(t),\tag{6}$$

$$\begin{aligned}\vartheta(t)=&\sum_{i=0}^{k_n-1}\alpha_{i+1,t}y_{r,t-i}+\sum_{i=0}^{k_n-1}\beta_{i+1,t}u(t-i-1)-y_{r,t+1}\\&+\varphi_{0,t}+\zeta(t+1\,|\,t)=\phi(t)+\zeta(t+1\,|\,t).\end{aligned}\tag{7}$$

Here, $|\vartheta(t)|$ is selected as an indicator of whether the system enters into the steady state because $|\vartheta(t)|$ should be zero if the system input $u(t)$ is perfect and the system output $y(t)$ is stable at the expected output y_r under the steady

state. To make $\{|\vartheta(t+j\,|\,t)|, j \geq 1\}$ be zero according to (6) and (7), one can design a sequence of "perfect" inputs $\{\overline{u}(t\,|\,t), \overline{u}(t+1\,|\,t), \ldots\}$ and the output deviations of the multistep-forward prediction $\{\overline{y}(t+j+1\,|\,t),\ j \geq 1\}$ of the model (4) satisfy

$$\begin{aligned}\overline{y}(t+j+1\,|\,t) = &\sum_{i=0}^{k_n-1} \alpha_{i+1,t+j}\overline{y}(t+j-i\,|\,t) \\ &+ \sum_{i=0}^{k_n-1} \beta_{i+1,t+j}\overline{u}(t+j-i\,|\,t),\end{aligned} \tag{8}$$

where if j is less than or equal to i, then $\overline{y}(t+j-i\,|\,t)$ is equal to $\overline{y}(t+j-i)$ and $\overline{u}(t+j-i\,|\,t)$ is equal to $\overline{u}(t+j-i)$. In this paper, model (8) is designed to satisfy the condition that the indicators $\{|\vartheta(t+j\,|\,t)|, j \geq 1\}$ are equal to zero. Next, to construct the system's state-space models based on the polynomial models (6) and (8), the state vector $\{X(t+j\,|\,t),\ j = 0, 1, 2, \ldots\}$ is selected as follows:

$$\begin{aligned}&X(t+j\,|\,t) = \left[x_{1,t+j|t}, x_{2,t+j\,|\,t}, \ldots, x_{k_n,t+j|t}\right]^{\mathrm{T}}, \\ &\begin{cases} x_{1,t+j|t} = \overline{y}(t+j\,|\,t), \\ x_{k,t+j|t} = \sum_{i=1}^{k_n+1-k} \alpha_{i+k-1,t+j-1}\overline{y}(t+j-i|t) + \sum_{i=1}^{k_n+1-k} \beta_{i+k-1,t+j-1}\overline{u}(t+j-i\,|\,t), \\ k = 2, 3, \ldots, k_n. \end{cases}\end{aligned} \tag{9}$$

Then, the system's state-space models can be obtained:

$$\begin{aligned}&X(t+1\,|\,t) = A_t X(t\,|\,t) + B_t\overline{u}(t\,|\,t) + \Xi(t), \\ &\begin{cases} A_t = \begin{bmatrix} \alpha_{1,t} & 1 & 0 & \cdots & 0 \\ \alpha_{2,t} & 0 & 1 & \cdots & \vdots \\ \vdots & \vdots & \vdots & \ddots & 0 \\ \alpha_{k_n-1,t} & 0 & 0 & \cdots & 1 \\ \alpha_{k_n,t} & 0 & 0 & \cdots & 0 \end{bmatrix}, \\ B_t = \begin{bmatrix} \beta_{1,t} \\ \beta_{2,t} \\ \vdots \\ \beta_{k_n,t} \end{bmatrix}, \\ \Xi(t) = \begin{bmatrix} \vartheta(t) \\ 0 \\ \vdots \\ 0 \end{bmatrix}, \end{cases}\end{aligned} \tag{10}$$

$$\begin{aligned}&X(t+j+1\,|\,t) = A_{t+j|t}X(t+j\,|\,t) + B_{t+j|t}\overline{u}(t+j\,|\,t), \\ &\begin{cases} A_{t+j\,|\,t} = \begin{bmatrix} \alpha_{1,t+j\,|\,t} & 1 & 0 & \cdots & 0 \\ \alpha_{2,t+j\,|\,t} & 0 & 1 & \cdots & \vdots \\ \vdots & \vdots & \vdots & \ddots & 0 \\ \alpha_{k_n-1,t+j\,|\,t} & 0 & 0 & \cdots & 1 \\ \alpha_{k_n,t+j\,|\,t} & 0 & 0 & \cdots & 0 \end{bmatrix}, \\ B_{t+j\,|\,t} = \begin{bmatrix} \beta_{1,t+j\,|\,t} \\ \beta_{2,t+j\,|\,t} \\ \vdots \\ \beta_{k_n,t+j\,|\,t} \end{bmatrix},\ j \geq 1. \end{cases}\end{aligned} \tag{11}$$

Since the state $s(t)$ is known at time t, the matrices A_t and B_t in (10) can be obtained; similarly, based on the system's history data, the state vector $X(t\,|\,t)$ in (10) can be obtained by (9). Considering that the vector $\Xi(t)$ in (10) contains a bounded unknown disturbance term $\zeta(t+1\,|\,t)$, it is obvious that the exact value of $\Xi(t)$ cannot be obtained at time t, but its variation range can be obtained. Here, the polytope Ω_Ξ that $\Xi(t)$ in (10) belongs to is constructed as follows:

$$\Omega_\Xi\colon \left\{\Xi(t) = \sum_{\tau=1}^{2} \lambda_{\tau,t}^{\Xi}\Xi_{t,\tau},\ \sum_{\tau=1}^{2} \lambda_{\tau,t}^{\Xi} = 1,\ \lambda_{\tau,t}^{\Xi} \geq 0\right\}, \tag{12}$$

where the vertices $\Xi_{t,1} = \left[\ (\phi(t) - \delta)\ \ 0\ \cdots\ 0\ \right]^{\mathrm{T}}$ and $\Xi_{t,2} = \left[\ (\phi(t) + \delta)\ \ 0\ \cdots\ 0\ \right]^{\mathrm{T}}$ and $\phi(t)$ is defined as in (7).

Remark 1. The coefficients $\left\{\alpha_{i+1,t+j|t}, \beta_{i+1,t+j|t} | i = 0, \ldots, k_n - 1;\ j \geq 1\right\}$ in (11) is established on the future working states $s(t+j\,|\,t)$. So, the future matrices $\left\{A_{t+j|t}, B_{t+j|t} | j \geq 1\right\}$ cannot be obtained. But, one can see that, if the varying region of every exponential term in $\alpha_{i+1,t+j|t}$ or $\beta_{i+1,t+j|t}$ can be found out, a polytope set can be built to cover the variation scope of the matrices $A_{t+j|t}$ or $B_{t+j|t}$ in (11).

Next, based on the time-varying coefficient information of the model (4), a method for constructing the convex polytope sets, which are used to cover the variation scope of the matrices $\left\{A_{t+j|t}, B_{t+j|t} | j \geq 1\right\}$, is designed.

2.1. Based on Parameter Upper and Lower Boundary Information. If only considering the boundary information of the parameters of the SD-ARX model (4), the convex polytopic sets can be constructed as follows:

$$\Omega_A:\left\{A_{t+j|t}=\sum_{a=1}^{2^m}\lambda_{a,t+j|t}^{\alpha}A_a,\ \sum_{a=1}^{2^m}\lambda_{a,t+j|t}^{\alpha}=1,\lambda_{a,t+j|t}^{\alpha}\geq 0\right\},$$
$$\Omega_B:\left\{B_{t+j|t}=\sum_{b=1}^{2^m}\lambda_{b,t+j|t}^{\beta}B_b,\ \sum_{b=1}^{2^m}\lambda_{b,t+j|t}^{\beta}=1,\lambda_{b,t+j|t}^{\beta}\geq 0\right\}, \tag{13}$$

where A_a and B_b are the vertices of Ω_A and Ω_B and

$$A_a=\begin{bmatrix}\kappa_{0,0}^{\alpha}+\sum_{h=1}^{m}\kappa_{0,h}^{\alpha}\left(\overline{\varepsilon}_{\alpha,h}\,\middle|\,\underline{\varepsilon}_{\alpha,h}\right) & 1 & 0 & \cdots & 0\\ \kappa_{1,0}^{\alpha}+\sum_{h=1}^{m}\kappa_{1,h}^{\alpha}\left(\overline{\varepsilon}_{\alpha,h}\,\middle|\,\underline{\varepsilon}_{\alpha,h}\right) & 0 & 1 & \cdots & 0\\ \vdots & \vdots & \vdots & \ddots & 0\\ \kappa_{k_\alpha-1,0}^{\alpha}+\sum_{h=1}^{m}\kappa_{k_\alpha-1,h}^{\alpha}\left(\overline{\varepsilon}_{\alpha,h}\,\middle|\,\underline{\varepsilon}_{\alpha,h}\right) & \vdots & \vdots & \cdots & \vdots\\ 0 & \vdots & \vdots & \cdots & 0\\ \vdots & \vdots & \vdots & \ddots & 0\\ 0 & 0 & 0 & \cdots & 1\\ 0 & 0 & 0 & \cdots & 0\end{bmatrix}_{k_n\times k_n}, \tag{14}$$

$$B_b=\begin{bmatrix}0\\ \vdots\\ 0\\ \kappa_{k_d,0}^{\beta}+\sum_{h=1}^{m}\kappa_{k_d,h}^{\beta}\left(\overline{\varepsilon}_{\beta,h}\,\middle|\,\underline{\varepsilon}_{\beta,h}\right)\\ \vdots\\ \kappa_{k_\beta+k_d-1,0}^{\beta}+\sum_{h=1}^{m}\kappa_{k_\beta+k_d-1,h}^{\beta}\left(\overline{\varepsilon}_{\beta,h}\,\middle|\,\underline{\varepsilon}_{\beta,h}\right)\\ 0\\ \vdots\\ 0\end{bmatrix}_{k_n\times 1}, \tag{15}$$

where $\left\{\kappa_{i,0}^{\alpha},\kappa_{i,h}^{\alpha}|h=1,\ldots,m;i=0,\ldots,k_\alpha-1\right\}$ and $\left\{\kappa_{i,0}^{\beta},\kappa_{i,h}^{\beta}|h=1,\ldots,m;i=k_d,\ldots,k_\beta+k_d-1\right\}$ are the linear parameters as in (4), the mark $(\overline{\varepsilon}_{\beta,h}|\underline{\varepsilon}_{\beta,h})$ indicates $\overline{\varepsilon}_{\alpha,h}$ or $\underline{\varepsilon}_{\alpha,h}$, the mark $(\overline{\varepsilon}_{\beta,h}|\underline{\varepsilon}_{\beta,h})$ indicates $\overline{\varepsilon}_{\beta,h}$ or $\underline{\varepsilon}_{\beta,h}$, and they are defined as follows:

$$\begin{cases}\varepsilon_h^{\alpha}(t)=e^{\left\{-\sigma_h^{\alpha}\left\|s(t)-\nu_h^{\alpha}\right\|_2^2\right\}},\\ \varepsilon_h^{\beta}(t)=e^{\left\{-\sigma_h^{\beta}\left\|s(t)-\nu_h^{\beta}\right\|_2^2\right\}},\\ \overline{\varepsilon}_{\alpha,h}=\max\left\{\varepsilon_h^{\alpha}(t),\forall s(t)\right\},\\ \underline{\varepsilon}_{\alpha,h}=\min\left\{\varepsilon_h^{\alpha}(t),\forall s(t)\right\},\\ \overline{\varepsilon}_{\beta,h}=\max\left\{\varepsilon_h^{\beta}(t),\forall s(t)\right\},\\ \underline{\varepsilon}_{\beta,h}=\min\left\{\varepsilon_h^{\beta}(t),\forall s(t)\right\},\end{cases} \tag{16}$$

where $\left\{\sigma_h^{\alpha},\sigma_h^{\beta},\nu_h^{\alpha},\nu_h^{\beta}|h=1,\ldots,m\right\}$ are the widths and centers of the neural networks as in (4) and $s(t)$ is the historical state data. From the boundary $[\underline{\varepsilon}_{\alpha,h},\overline{\varepsilon}_{\alpha,h}]$ or $[\underline{\varepsilon}_{\beta,h},\overline{\varepsilon}_{\beta,h}]$ in (16) and the coefficients of regression structure with m exponential terms as in (4), 2^m vertices A_a or B_b of the set Ω_A or Ω_B can be obtained from (14) or (15). So, the polytopic LPV model (11) can be constructed.

Remark 2. Considering that the matrices $\left\{A_{t+1|t},B_{t+1|t}\right\}$ in (11) may not reach to the boundary of the sets $\{\Omega_A,\Omega_B\}$ directly in only one step, in this paper, the variation range information of the SD-ARX model's parameters is further considered to compress the size of the convex polytopic sets $\{\Omega_A,\Omega_B\}$. Thus, the size of $\{\Omega_A,\Omega_B\}$, which is built to wrap the matrices $\left\{A_{t+1|t},B_{t+1|t}\right\}$ in (11), can be greatly compressed. Moreover, it may reduce the conservativeness of subsequent robust predictive controller and improve its control performance.

2.2. Based on Parameter Variation Rate Information. By using the parameter variation rate information of the SD-ARX model (4), the convex polytopic sets used to wrap the state matrices $\left\{A_{t+1|t},B_{t+1|t}\right\}$ are designed as

$$\Omega_C:\left\{\mathrm{A}_{t+1|t}=\sum_{c=1}^{2^m}\lambda_{c,t+1|t}^{\alpha}C_c,\ \sum_{c=1}^{2^m}\lambda_{c,t+1|t}^{\alpha}=1,\ \lambda_{c,t+1|t}^{\alpha}\geq 0\right\},$$
$$\Omega_D:\left\{B_{t+1|t}=\sum_{d=1}^{2^m}\lambda_{d,t+1|t}^{\beta}D_d,\ \sum_{d=1}^{2^m}\lambda_{d,t+1|t}^{\beta}=1,\ \lambda_{d,t+1|t}^{\beta}\geq 0\right\}, \tag{17}$$

where C_c and D_d are the vertices of Ω_C and Ω_D and the basic structure of C_c or D_d is the same as that of A_a or B_b in (14) or (15), except that the calculation method for the item $(\overline{\varepsilon}_{\alpha,h}|\underline{\varepsilon}_{\alpha,h})$ or $(\overline{\varepsilon}_{\beta,h}|\underline{\varepsilon}_{\beta,h})$ in (14) or (15) is different. In order to facilitate the difference, here we redefine the item $(\overline{\varepsilon}_{\alpha,h}|\underline{\varepsilon}_{\alpha,h})$ or $(\overline{\varepsilon}_{\beta,h}|\underline{\varepsilon}_{\beta,h})$ of the vertex C_c or D_d as $(\overleftrightarrow{\varepsilon}_{\alpha,h}|\underline{\varepsilon}_{\alpha,h})$ or $(\overleftrightarrow{\varepsilon}_{\beta,h}|\underline{\varepsilon}_{\beta,h})$. In this paper, the item $(\overleftrightarrow{\varepsilon}_{\alpha,h}|\underline{\varepsilon}_{\alpha,h})$ or $(\overleftrightarrow{\varepsilon}_{\beta,h}|\underline{\varepsilon}_{\beta,h})$ in the vertex C_c or D_d is calculated by the following strategy:

$$\begin{cases}\left(\overleftrightarrow{\varepsilon}_{\alpha,h}\,\middle|\,\underline{\varepsilon}_{\alpha,h}\right)=\overleftrightarrow{\varepsilon}_{\alpha,h}\text{ or }\underline{\varepsilon}_{\alpha,h},\\ \varepsilon_{\alpha,h}=\min\left\{\overline{\varepsilon}_{\alpha,h},\varepsilon_h^{\alpha}(t)+\Delta\overline{\varepsilon}_{\alpha,h}\right\},\\ \underline{\varepsilon}_{\alpha,h}=\max\left\{\underline{\varepsilon}_{\alpha,h},\varepsilon_h^{\alpha}(t)+\Delta\underline{\varepsilon}_{\alpha,h}\right\},\\ \Delta\overline{\varepsilon}_{\alpha,h}=\max\left\{-2\sigma_h^{\alpha}\left(s(t)-\nu_h^{\alpha}\right)^{\mathrm{T}}\varepsilon_h^{\alpha}(t)\Delta s(t),\forall s(t)\right\},\\ \Delta\underline{\varepsilon}_{\alpha,h}=\min\left\{-2\sigma_h^{\alpha}\left(s(t)-\nu_h^{\alpha}\right)^{\mathrm{T}}\varepsilon_h^{\alpha}(t)\Delta s(t),\forall s(t)\right\},\end{cases} \tag{18}$$

$$\begin{cases} \left(\overleftrightarrow{\varepsilon}_{\beta,h} \,\middle|\, \underleftrightarrow{\varepsilon}_{\beta,h}\right) = \overleftrightarrow{\varepsilon}_{\beta,h} \text{ or } \underleftrightarrow{\varepsilon}_{\beta,h}, \\ \overleftrightarrow{\varepsilon}_{\beta,h} = \min\left\{\overline{\varepsilon}_{\beta,h}, \varepsilon_h^{\beta}(t) + \Delta\overline{\varepsilon}_{\beta,h}\right\}, \\ \underleftrightarrow{\varepsilon}_{\beta,h} = \max\left\{\underline{\varepsilon}_{\beta,h}, \varepsilon_h^{\beta}(t) + \Delta\underline{\varepsilon}_{\beta,h}\right\}, \\ \Delta\overline{\varepsilon}_{\beta,h} = \max\left\{-2\sigma_h^{\beta}\left(s(t) - \nu_h^{\beta}\right)^{\mathrm{T}}\varepsilon_h^{\beta}(t)\Delta s(t), \forall s(t)\right\}, \\ \Delta\underline{\varepsilon}_{\beta,h} = \min\left\{-2\sigma_h^{\beta}\left(s(t) - \nu_h^{\beta}\right)^{\mathrm{T}}\varepsilon_h^{\beta}(t)\Delta s(t), \forall s(t)\right\}, \end{cases} \tag{19}$$

where the marks $\{\overline{\varepsilon}_{j,h}, \underline{\varepsilon}_{j,h}, \varepsilon_h^j(t), \sigma_h^j, \nu_h^j | h = 1, \ldots, m; j = \alpha, \beta\}$ have been defined in (16) and $s(t)$ is the historical state data, and $\Delta s(t)$ is the variation rate of $s(t)$. From the boundary $[\underleftrightarrow{\varepsilon}_{\alpha,h}, \overleftrightarrow{\varepsilon}_{\alpha,h}]$ or $[\underleftrightarrow{\varepsilon}_{\beta,h}, \overleftrightarrow{\varepsilon}_{\beta,h}]$ in (18) or (19) and the coefficients of regression structure with m exponential terms as in (4), 2^m vertices C_c or D_d can be obtained. And then, the convex polytopic set Ω_C or Ω_D, which is used to wrap state matrix $A_{t+1|t}$ or $B_{t+1|t}$, can be built.

Remark 3. Based on the time-varying coefficient information of the SD-ARX model, the state-space model (10) is built to represent the system's current behavior, and the polytopic state-space model (11) is constructed to wrap the future dynamics of the system. Note that, there is no need to make such assumption that the bounds on the parameter's variation range in the system's model are available. In this paper, the polytopic state-space model is constructed directly based on the special structure of the SD-ARX model itself.

Next, based on the established models (10) and (11), a two-stage scheduling robust controller is designed.

3. Robust Predictive Controller Design Process

MPC is a model-based computer optimization control method, which makes prediction about the system's future behavior using dynamic model. In this subsection, based on models (10) and (11), which the system's dynamics is forced in, an RPC algorithm is designed. The objective function of the RBF-ARX model-based RPC (RBF-ARX-RPC) algorithm is designed as follows:

$$\min_{\overline{u}(t+j|t), j=0,1,2,\ldots} \max_{\substack{\Xi(t)\in\Omega_\Xi,\, A_{t+1|t}\in\Omega_C, B_{t+1|t}\in\Omega_D, \\ A_{t+j|t}\in\Omega_A, B_{t+j|t}\in\Omega_B,\, j\geq 2.}} J_0^{\infty}(t) = \sum_{j=0}^{\infty}\left\{X(t+j|t)^{\mathrm{T}}WX(t+j|t) + \overline{u}(t+j|t)^{\mathrm{T}}R\overline{u}(t+j|t)\right\}, \tag{20}$$

$$\text{s.t.} \quad (10), (11), |\overline{u}(t+j|t)| \leq \overline{u}_{\max}, j \geq 0; u_{\min} \leq u(t|t) \leq u_{\max}; |\overline{y}(t+i|t)| \leq \overline{y}_{\max}, i \geq 1,$$

where $R = R^{\mathrm{T}} > 0$ and $W = W^{\mathrm{T}} \geq 0$ are the weight coefficients; $\overline{u}(t+j|t)$ is the predicted input increment at $t+j$; $\overline{u}(t+j|t)$ and $\overline{y}(t+i|t)$ are imposed with constraints $|\overline{u}(t+j|t)| \leq \overline{u}_{\max}$ and $|\overline{y}(t+i|t)| \leq \overline{y}_{\max}$, respectively; and $u(t|t)$ is the control law at time t and is constrained by $u_{\min} \leq u(t|t) \leq u_{\max}$.

To design the two-stage scheduling RPC algorithm, first, $J_0^{\infty}(t)$ in (20) is divided into three parts: $J_0^{\infty}(t) = J_0^1(t) + J_1^2(t) + J_2^{\infty}(t)$, where $J_0^1(t) = X(t|t)^{\mathrm{T}}WX(t|t) + \overline{u}(t|t)^{\mathrm{T}}R\overline{u}(t|t)$, $J_1^2(t) = X(t+1|t)^{\mathrm{T}}WX(t+1|t) + \overline{u}(t+1|t)^{\mathrm{T}}R\overline{u}(t+1|t)$, and $J_2^{\infty}(t)$ is the remaining part of the objective function $J_0^{\infty}(t)$. And, in the objective function (20), $\overline{u}(t|t)$ and $\overline{u}(t+1|t)$ are free decision variables, and the input increments $\{\overline{u}(t+j|t) | j \geq 2\}$ are calculated by $\overline{u}(t+j|t) = F(t)X(t+j|t)$, in which the matrix $F(t)$ can be determined at time t. And then, the LMI synthesis method is used to settle the infinite horizon optimization problem (20).

First, the quadratic function of state vector is defined as follows:

$$\Upsilon(j,t) = X(t+j|t)^{\mathrm{T}}P(j,t)X(t+j|t), \quad j \geq 2, \tag{21}$$

where $P(j,t)$ is a positive definite matrix. And, for any $A_{t+j|t} \in \Omega_A$ and $B_{t+j|t} \in \Omega_B$, $j \geq 2$, we suppose $\Upsilon(j,t)$ at time t satisfies

$$\begin{aligned} \Upsilon(j+1,t) - \Upsilon(j,t) \leq -\big\{&X(t+j|t)^{\mathrm{T}}WX(t+j|t) \\ &+ \overline{u}(t+j|t)^{\mathrm{T}}R\overline{u}(t+j|t)\big\}. \end{aligned} \tag{22}$$

Next, one can get the following inequality by summing (22) from $j = 2$ to ∞:

$$\max_{A_{t+j|t}\in\Omega_A, B_{t+j|t}\in\Omega_B, j\geq 2} \quad J_2^{\infty}(t) < \Upsilon(2,t). \tag{23}$$

And then, optimization problem (20) can be converted as follows:

$$\min_{\overline{u}(t|t), \overline{u}(t+1|t), P(2,t).} J_0^1(t) + J_1^2(t) + \Upsilon(2,t), \tag{24}$$

$$\text{s.t.} \quad (10), (11), (25), |\overline{u}(t+j|t)| \leq \overline{u}_{\max}, j \geq 0; u_{\min} \leq u(t|t) \leq u_{\max}; |\overline{y}(t+i|t)| \leq \overline{y}_{\max}, i \geq 1.$$

In this paper, the Lyapunov matrices $\{P_{ab}|a,b=1,2,\ldots,2^m\}$ are used to build the time-varying Lyapunov matrices $P(j,t)=\sum_{a=1}^{2^m}\lambda_{a,t+j|t}^{\alpha}\sum_{b=1}^{2^m}\lambda_{b,t+j|t}^{\beta}P_{ab}$ for $j\geq 2$. If the Lyapunov matrices P_{ab} exist, the minimization problem (24) can then be settled by Theorem 1.

Theorem 1. *The min-max optimization problem (20), which is designed to find $\overline{u}(t\mid t)$, $\overline{u}(t+1\mid t)$, and the feedback gain $F(t)$, can be settled by the following semidefinite programming:*

$$\min_{\gamma,\overline{u}(t\mid t),\overline{u}(t+1\mid t),Q_{ab},Y,G,Z,K}\quad \gamma, \tag{25}$$

subject to

$$\begin{bmatrix} 1 & * & * & * & * & * & * & * \\ C_c\left(A_tX(t\mid t)+B_t\overline{u}(t\mid t)+\Xi_{t,\tau}\right)+D_d\overline{u}(t+1\mid t) & Q_{ab} & * & * & * & * & * & * \\ 0 & 0 & I & * & * & * & * & * \\ 0 & 0 & 0 & I & * & * & * & * \\ W^{1/2}X(t\mid t) & 0 & 0 & 0 & \gamma I & * & * & * \\ R^{1/2}\overline{u}(t\mid t) & 0 & 0 & 0 & 0 & \gamma I & * & * \\ W^{1/2}\left(A_tX(t\mid t)+B_t\overline{u}(t\mid t)+\Xi_{t,\tau}\right) & 0 & 0 & 0 & 0 & 0 & \gamma I & * \\ R^{1/2}\overline{u}(t+1\mid t) & 0 & 0 & 0 & 0 & 0 & 0 & \gamma I \end{bmatrix}\geq 0, \tag{26}$$

$$\begin{bmatrix} G+G^T-Q_{ab} & * & * & * \\ A_aG+B_bY & Q_{ef} & * & * \\ W^{1/2}G & 0 & \gamma I & * \\ R^{1/2}Y & 0 & 0 & \gamma I \end{bmatrix}\geq 0, \tag{27}$$

and with the following variable constraints,

$$\begin{aligned} |\overline{u}(t\mid t)|&\leq \overline{u}_{\max},\\ |\overline{u}(t+1\mid t)|&\leq \overline{u}_{\max},\\ u_{\min}\leq u(t\mid t)&\leq u_{\max},\\ \begin{bmatrix} Z & Y \\ Y^{\mathrm{T}} & G+G^{\mathrm{T}}-Q_{ab}\end{bmatrix}&\geq 0,\quad Z_{ii}\leq \overline{u}_{\max}^2; \end{aligned} \tag{28}$$

$$\begin{aligned} \left|C\left(A_tX(t\mid t)+B_t\overline{u}(t\mid t)+\Xi_{t,\tau}\right)\right|&\leq \overline{y}_{\max},\\ \left|C\left(C_c\left(A_tX(t\mid t)+B_t\overline{u}(t\mid t)+\Xi_{t,\tau}\right)+D_d\overline{u}(t+1\mid t)\right)\right|&\leq \overline{y}_{\max},\\ \begin{bmatrix} K & C(A_aG+B_bY) \\ (A_aG+B_bY)^{\mathrm{T}}C^{\mathrm{T}} & G+G^{\mathrm{T}}-Q_{ab}\end{bmatrix}&\geq 0,\quad K_{jj}\leq \overline{y}_{\max}^2, \end{aligned} \tag{29}$$

where $a,b,c,d,e,f=1,2,\ldots,2^m$; $\tau=1,2$; the symbol $*$ indicates a symmetric structure; $Q_{ab}=\gamma P_{ab}^{-1}>0$; the feedback gain matrix is defined as $F(t)=YG^{-1}$; Z and K are the symmetric matrices, Z_{ii} is the i-th diagonal element of the symmetric matrix Z, and K_{jj} is the j-th diagonal element of the symmetric matrix K. In the above (26)–(29), A_t, B_t, $X(t\mid t)$, A_a, B_b, C_c, D_d, and $\Gamma_{t,\tau}$ can be calculated by model (4) at time t and the historical data of the system.

Proof. Substituting the state-space model (11), $\overline{u}(t+j\mid t)=F(t)X(t+j\mid t)$ and (21) into (22), one can get the following inequality:

$$\begin{aligned} &\left[A_{t+j|t}+B_{t+j|t}F(t)\right]^{\mathrm{T}}P(j+1,t)\left[A_{t+j|t}+B_{t+j|t}F(t)\right]\\ &\quad -P(j,t)+F(t)^{\mathrm{T}}RF(t)+W\leq 0. \end{aligned} \tag{30}$$

Next, it can be verified that the inequality (30) is satisfied if and only if the Lyapunov matrices $\{P_{ab}\mid a,b=1,2,\ldots,2^m\}$, which are used to build the time-varying Lyapunov matrices $P(j,t)=\sum_{a=1}^{2^m}\lambda_{a,t+j|t}^{\alpha}\sum_{b=1}^{2^m}\lambda_{b,t+j\mid t}^{\beta}P_{ab}$ for $j\geq 2$, exist, and

$$\left[A_a+B_bF(t)\right]^{\mathrm{T}}P_{ef}\left[A_a+B_bF(t)\right]-P_{ab}+F(t)^{\mathrm{T}}RF(t)+W\leq 0. \tag{31}$$

By using the Schur complement [35] and defining $Q_{ab} = \gamma P_{ab}^{-1}$, $Q_{ef} = \gamma P_{ef}^{-1}$, $F(t) = YG^{-1}$, the inequality (31) can then be converted to the inequality (27).

Therefore, the optimization problem (24) can be converted as follows:

$$\begin{aligned} &\min_{\gamma, \overline{u}(t\mid t), \overline{u}(t+1\mid t), Q_{ab}, Y, G} \gamma, \\ &\text{s.t.} \quad (10), (11), (29), J_0^1(t) + J_1^2(t) + \Upsilon(2,t) \le \gamma, \\ &\quad |\overline{u}(t+j\mid t)| \le \overline{u}_{\max},\ j \ge 0;\ u_{\min} \le u(t\mid t) \le u_{\max}; \\ &\quad |\overline{y}(t+i\mid t)| \le \overline{y}_{\max}, i \ge 1, \end{aligned} \tag{32}$$

where γ is a suitable nonnegative scalar.

According to (24) and introducing (10) and (11) into (32), one can obtain that

$$J_0^1(t) + J_1^2(t) + X(t+2\mid t)^{\mathrm{T}} P_{ab} X(t+2\mid t) \le \gamma, \tag{33}$$

where the state $X(t+1\mid t)$ in $J_1^2(t)$ is defined in (10) and the vector $\Xi(t)$ belongs to Ω_Ξ; the state $X(t+2\mid t)$ is defined in (11), and the state matrix $A_{t+1\mid t}$ or $B_{t+1\mid t}$ belongs to Ω_C or Ω_D, respectively. And then, by using the Schur complement [35], inequality (33) can be finally converted to the LMIs (26).

The variable constraints in (24) can also be converted to the LMIs. First, separate the variables into three parts: $\overline{U}_0^\infty = \left\{\overline{u}(t\mid t), \overline{u}(t+1\mid t), \overline{U}_2^\infty\right\}$ and $\overline{Y}_1^\infty = \{\overline{y}(t+1\mid t), \overline{y}(t+2\mid t), \overline{Y}_3^\infty\}$. Then each constraint is imposed on each part. Similar to Ref. [35], the incremental constraints contained in (36) can ultimately be represented as LMI (28) and (29).

Hence, the two-stage scheduling RPC optimization problem established based on (10), (11), and (20) is finally converted to $\min_{\gamma, \overline{u}(t\mid t), \overline{u}(t+1\mid t), Q_{ab}, Y, G, Z, K} \gamma$, subject to the LMIs (26)–(29). □

Remark 4. Although both $\overline{u}(t\mid t)$ and $\overline{u}(t+1\mid t)$ are computed at each sampling time, the control action implemented on the controlled system is only $u(t) = \overline{u}(t\mid t) + u(t-1)$, and this calculation process is repeated at the next sampling time.

According to the conclusion shown in Theorem 1, the result similar to Theorem 3 in Ref. [6] can be obtained:

Theorem 2. *When Theorem 1 is executed in a receding horizon fashion, the feasibility of the minimization problem (25) guarantees stability.*

Remark 5. The main idea behind the two-stage scheduling RPC algorithm is to separate the second-stage cost $J_1^2(t)$ in addition to the first-stage cost $J_0^1(t)$ from the objective function $J_0^\infty(t)$, so as to relax more control moves from the constant feedback control law.

Remark 6. It is different to the one-stage scheduling RPC algorithms [28, 29], in which only the first control increment $\overline{u}(t\mid t)$ is separated from the future control series, and all other future control actions are in feedback forms with constant feedback gains. In the two-stage scheduling RPC algorithm, in addition to $\overline{u}(t\mid t)$, the control increment $\overline{u}(t+1\mid t)$ is also separated from the future control series and is acted as a free control variable to increase the degree of freedom of the control.

Table 1: Parameters of the water tank system.

Cross section of Tank 1	$S_1 = 500\,\mathrm{cm}^2$
Cross section of Tank 2	$S_2 = 360\,\mathrm{cm}^2$
Scaling factor	$\pi_1 = 0.05\,\mathrm{cm}^3/\mathrm{s} - \mathrm{v}$
Water density	$\mu = 0.001\,\mathrm{kg/cm}^3$
Outlet hole section of Tank 1	$A_1 = 9\,\mathrm{cm}^2$
Outlet hole section of Tank 2	$A_2 = 8.5\,\mathrm{cm}^2$
Gravity constant	$g = 980\,\mathrm{cm/s}^2$

4. Case Study

The modeling and control of a water tank system is provided in this section to illustrate the performance of the two-stage scheduling RPC algorithm. Level control of the water tank system is often used in literatures [36, 37] for comparison study. The mass and energy balance equations for the water tank system [36] are as follows:

$$\begin{cases} \dfrac{\mathrm{d}H_1}{\mathrm{d}t} = -\dfrac{A_1}{S_1}\sqrt{2gH_1} + \dfrac{\pi_1}{\mu S_1}U, \\ \dfrac{\mathrm{d}H_2}{\mathrm{d}t} = \dfrac{A_1}{S_2}\sqrt{2gH_1} - \dfrac{A_2}{S_2}\sqrt{2gH_2}, \end{cases} \tag{34}$$

where U is the control voltage of the pump and H_1 and H_2 are the liquid levels of the two tanks; the related parameters of the water tank system are shown in Table 1. In this case study, the control problem is to control the level $H_2(t)$ of the lower tank by adjusting the input voltage $U(t)$ of the pump.

4.1. Modeling for Water Tank System. The modeling method in Section 2 is used to identify the characteristics of the water tank system. First, the basic SD-ARX model is designed as follows:

$$\begin{aligned} H_2(t+1) &= \varphi_0(s(t)) + \sum_{i=0}^{k_\alpha - 1} \varphi_{\alpha,i}(s(t)) H_2(t-i) \\ &\quad + \sum_{i=k_d}^{k_\beta + k_d - 1} \varphi_{\beta,i}(s(t)) U(t-i) + \xi(t+1), \\ \begin{cases} \varphi_0(s(t)) = \kappa_0^0 + \sum_{h=1}^{m} \kappa_h^0 e^{\left\{-\sigma_h^\alpha \left\| s(t) - \nu_h^\alpha \right\|_2^2\right\}}, \\ \varphi_{j,i}(s(t)) = \kappa_{i,0}^j + \sum_{h=1}^{m} \kappa_{i,h}^j e^{\left\{-\sigma_h^j \left\| s(t) - \nu_h^j \right\|_2^2\right\}}, \\ \nu_h^j = \left[\nu_{h,1}^j, \nu_{h,2}^j, \ldots, \nu_{h,d}^j\right]^{\mathrm{T}}, \\ j = \alpha, \beta, \end{cases} \end{aligned} \tag{35}$$

where the input voltage $U(t)$ and liquid level $H_2(t)$ are the input and output, respectively; k_α, k_β, k_d, m, and d are the orders; the state vector of the system is designed as $s(t) = [H_2(t), \ldots, H_2(t-d+1)]^{\mathrm{T}}$ because the nonlinearity of the system is mainly caused by the change of the liquid level of

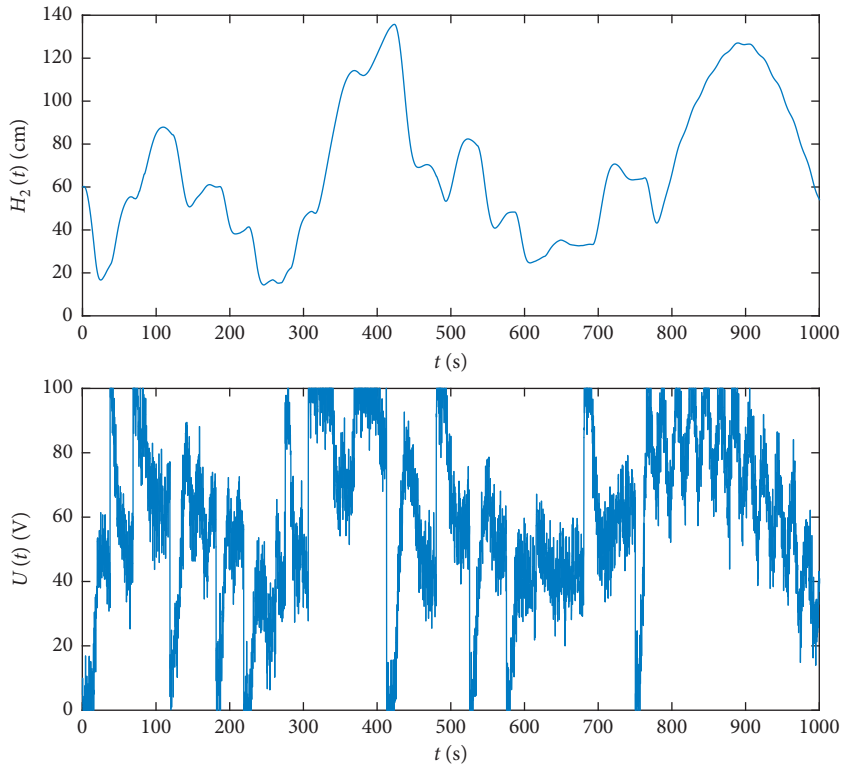

Figure 1: Output and input data of the water tank system.

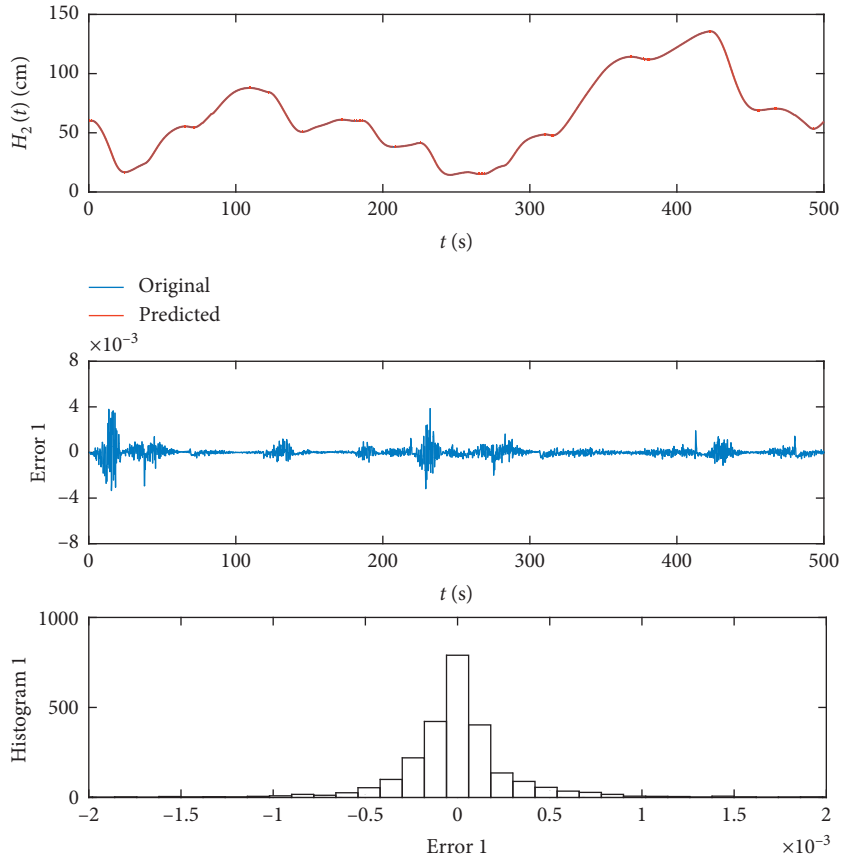

Figure 2: Actual and predicted output, predicted error, and its histogram for training data.

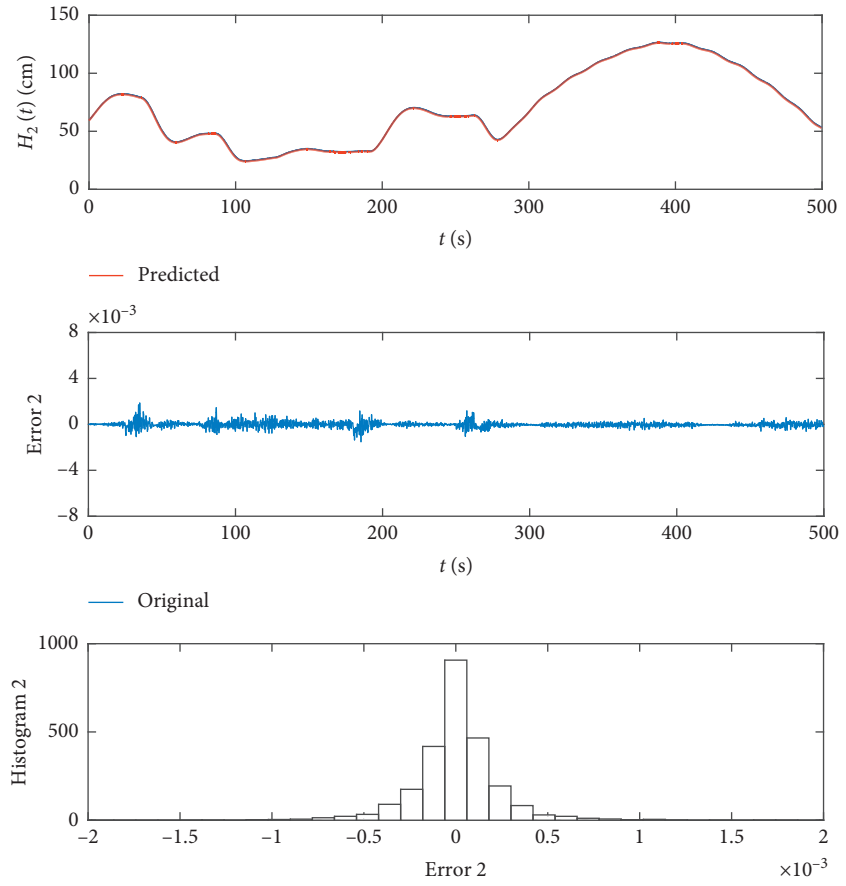

Figure 3: Actual and predicted output, predicted error, and its histogram for testing data.

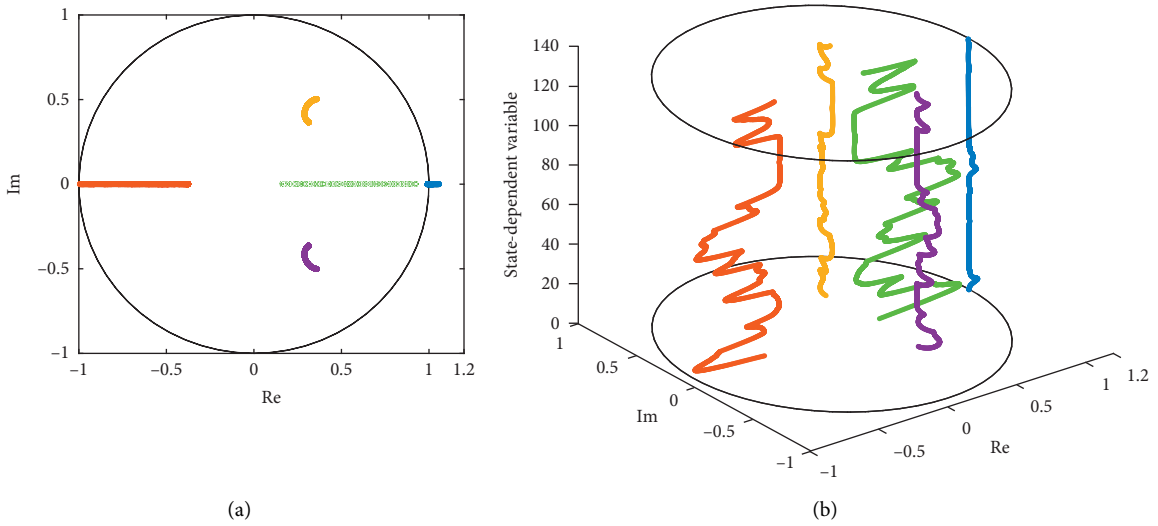

Figure 4: State-space model' poles varying with the state $s(t)$.

the Tank 2; and the linear parameters $\theta_L = \{\kappa_0^0, \kappa_h^0, \kappa_{i,0}^j, \kappa_{i,h}^j\}$ and nonlinear parameters $\theta_N = \{\sigma_h^j, \nu_h^j\}$ in model (35) are optimized by the R-SNPOM [22]. The detailed optimization process of the nonlinear parameters and linear parameters can be found in Ref. [22], which is omitted here.

In identification modeling, to fully excite the dynamics of the water tank system, the modeling data of the system is sampled under a PID controller. The period of the identification data collection in this modeling process is 0.2 s. And, the identification data of the water tank system are finally selected as shown in Figure 1, in which the first 2500 data are

Table 2: Controller parameters.

Algorithms	PID-M	RBF-ARX-TRPC and RBF-ARX-RPC
Controller parameters	1: $K_p = 40, K_i = 0.1, K_d = 20$; 2: $K_p = 80, K_i = 0.03, K_d = 20$; 3: $K_p = 60, K_i = 0.08, K_d = 20$.	$R = 0.001, W = 1$.
Variable constraints	$u_{\min} = 2, u_{\max} = 100$.	$u_{\min} = 2, u_{\max} = 100, \overline{u}_{\max} = 150$.

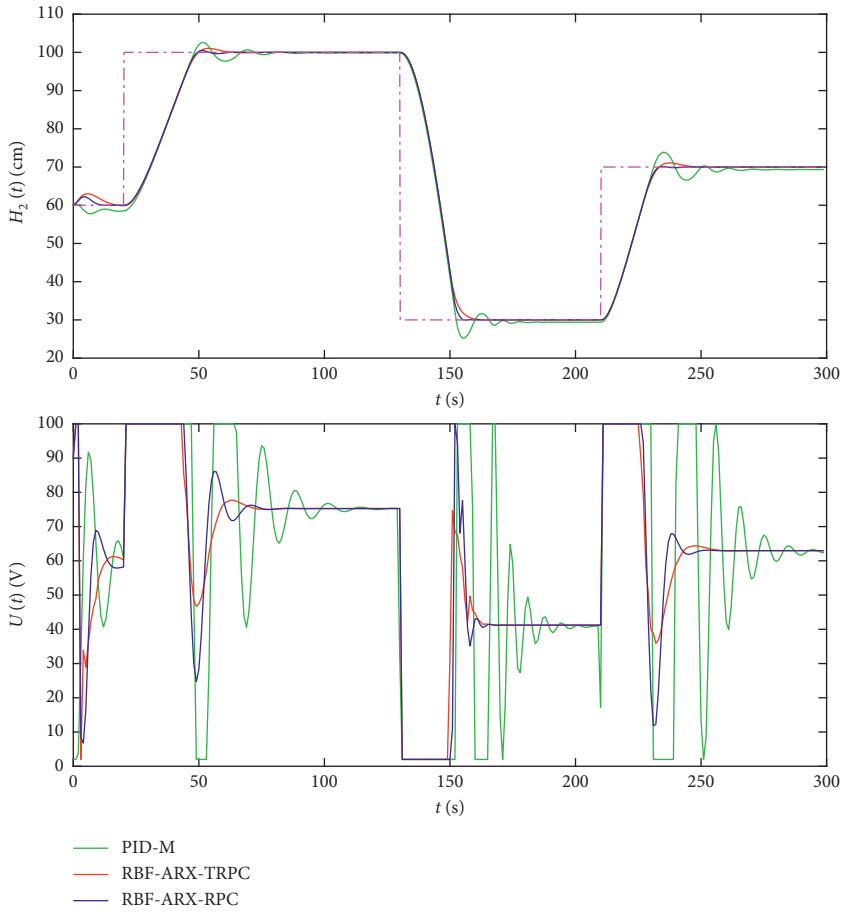

Figure 5: Trajectory tracking performances without external disturbance.

used for training and the next 2500 are used for testing. In this paper, the AIC value is selected as the main evaluation standard to determine the orders of the SD-ARX model (35). The orders of the final suitable SD-ARX model are selected as $k_\alpha = 5$, $k_\beta = 4$, $k_d = 1$, $m = 1$, and $d = 2$.

Figures 2 and 3 show the comparison between the actual output and the predicted output of the model (35), predicted error, and its histogram for the training data and testing data, respectively. From Figures 2 and 3, it is clearly seen that the predicted errors of the model (35) are only within the range of −0.004 cm to +0.004 cm and they are almost Gaussian distribution. It indicates that the identified SD-ARX model (35) has good modeling accuracy.

Next, by defining the system deviation variables (5) and the state vector (9), the model (10) of the water tank system at each sampling instant can be obtained just as described in Section 2. Figure 4 shows the poles of the state-space model (10) varying with the state $s(t)$. The different color in Figure 4 denotes the different pole.

From Figure 4, one can see that the dynamics of the water tank system vary obviously with the state $s(t)$. So, based on the variation range information of the state $s(t)$ in the SD-ARX model (35), the polytopic state-space models (10) and (11) can be designed to wrap the future dynamics of the water tank system. In this paper, based on the parameters' boundary information of the identified model (35), the vertices of convex polytopic sets $\{\Omega_A, \Omega_B\}$, i.e., A_a and B_b, can be obtained according to the (14) and (15), where $\overline{\varepsilon}_{\alpha,h}$, $\underline{\varepsilon}_{\alpha,h}$, $\overline{\varepsilon}_{\beta,h}$, and $\underline{\varepsilon}_{\beta,h}$ are calculated by (16) on the basis of the identification data shown in Figure 1. Moreover, based on the parameters' variation rate information of the identified model (35), the vertices of convex polytopic sets $\{\Omega_C, \Omega_D\}$, i.e., C_c and D_d, can be obtained according to (18) and (19),

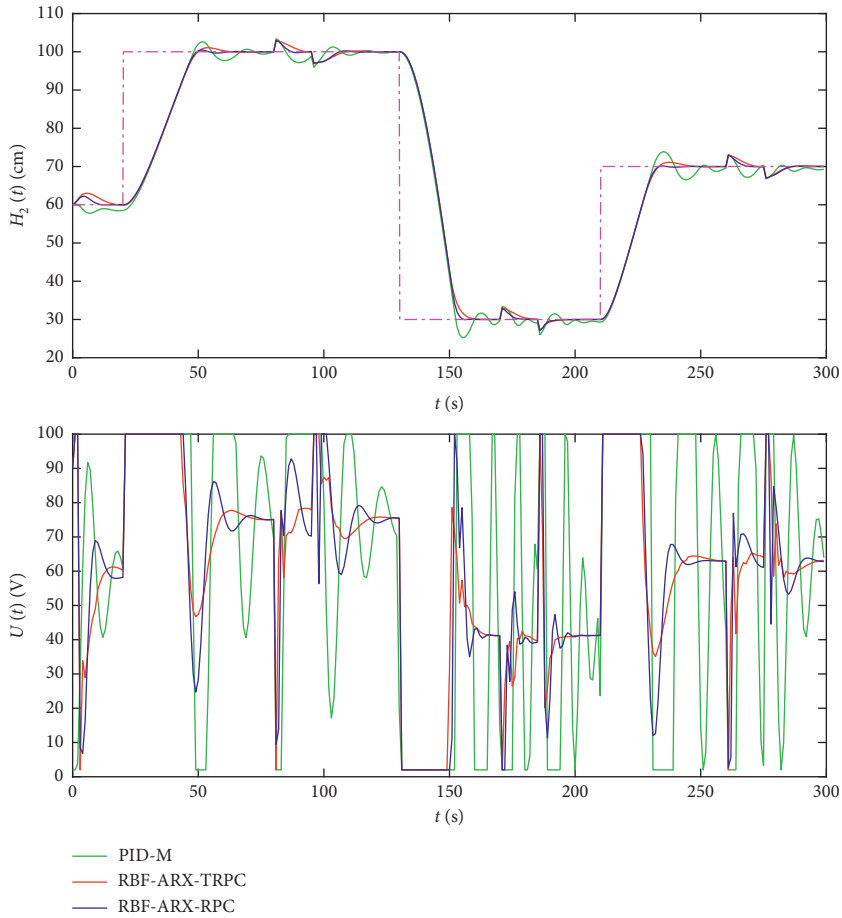

Figure 6: Disturbance rejection performances with forward square wave disturbance.

where $\overleftrightarrow{\varepsilon}_{\alpha,h}$, $\underleftrightarrow{\varepsilon}_{\alpha,h}$, $\overleftrightarrow{\varepsilon}_{\beta,h}$, and $\underleftrightarrow{\varepsilon}_{\beta,h}$ are calculated by (18) and (19). So, the state-space models (10) and (11) can be finally obtained.

4.2. Control Results and Analysis. The trajectory tracking and disturbance rejection experiments are carried out on the water tank system in this subsection. The simulation experiments are carried out in Matlab 2017b software, the LMI control toolbox in Simulink is used to settle the robust optimization problem, and the sampling period of the control system is 1.5 second. For comparison, two other algorithms, which are the well-tuned PID with multiple sets of parameters (PID-M) and the RBF-ARX model-based RPC algorithm proposed in Ref. [30] (RBF-ARX-TRPC), are also carried out.

To obtain better PID control performance, we use three different PIDs to control three step responses of the system (steps from 60 cm to 100 cm, 100 cm to 30 cm, and 30 cm to 70 cm, respectively). In this paper, the well-tuned parameters of each PID, which are selected through trial and error, are shown in Table 2. For fair comparison, the RBF-ARX-TRPC algorithm and the proposed RBF-ARX-RPC algorithm are all based on the same model, which is identified in Section 4.1. The controller parameters and variable constraints of the three algorithms are all given in Table 2.

Figure 5 shows the trajectory tracking performances of the three algorithms (PID-M, RBF-ARX-TRPC [30], and RBF-ARX-RPC proposed in this paper). In Figure 5, the pink dotted line denotes the desired trajectory of the liquid level of the lower tank $H_2(t)$, and it increases from 60 cm to 100 cm at the 20$^{\text{th}}$ second, decreases from 100 cm to 30 cm at the 130$^{\text{th}}$ second, and then increases from 30 cm to 70 cm at the 210$^{\text{th}}$ second.

From Figure 5, one can see that the trajectory tracking performance of the PID-M has greater overshoot and longer adjustment time than the RBF-ARX-TRPC [30] and RBF-ARX-RPC, whether in the ascending or descending phase. Meanwhile, it is clearly seen that the trajectory tracking performance of the RBF-ARX-RPC proposed in this paper has smaller overshoot and shorter adjustment time than the other two algorithms.

To verify the algorithms' disturbance rejection ability, the anti-jamming experiments are carried out. Figures 6 and 7 show the disturbance rejection performances of the three algorithms with forward or reverse square wave disturbance. In Figure 6, a forward square wave disturbance with an amplitude of 3 cm and a duration of 15 seconds is added into the liquid level of the lower tank $H_2(t)$ at the 80-th second, the 170-th second, and the 260-th second, respectively. Similarly, in Figure 7, a reverse square wave disturbance with an amplitude of −3 cm and a duration of 15 seconds is added into the liquid

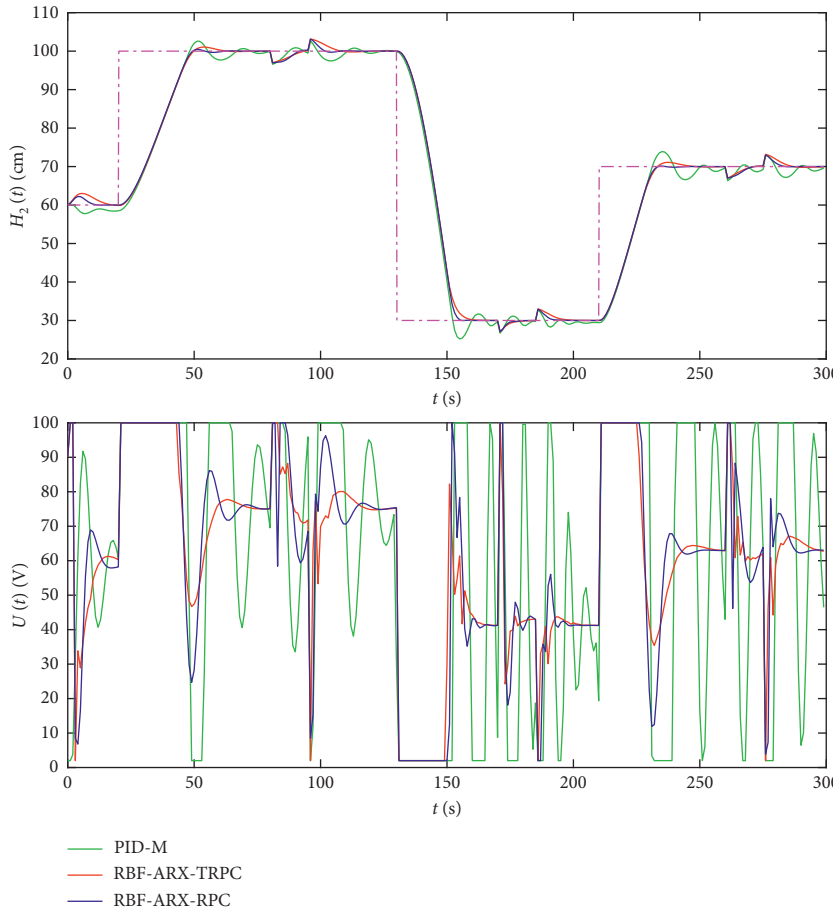

Figure 7: Disturbance rejection performances with reverse square wave disturbance.

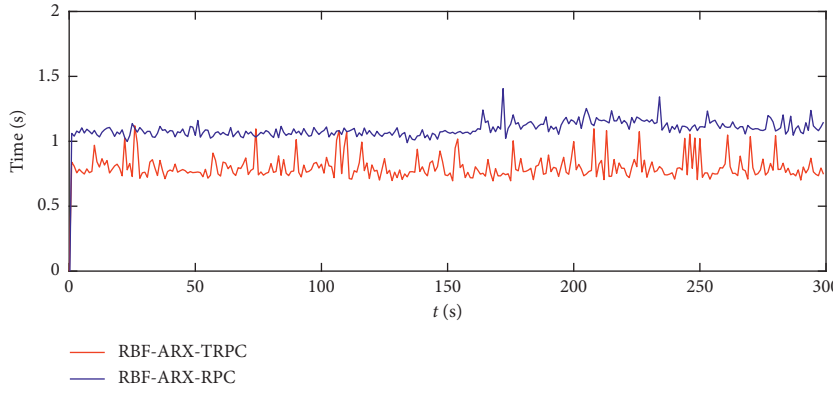

Figure 8: Real-time computation times of the two RPC algorithms.

level of the lower tank $H_2(t)$ at the 80-th second, the 170-th second, and the 260-th second, respectively.

From Figures 6 and 7, one can see that the anti-jamming result of the PID-M is the worst. The RBF-ARX-TRPC [30] has a certain degree of anti-jamming ability, and the result is better than the PID-M. The result of the RBF-ARX-RPC is the best, especially when there is external interference. As shown in Figure 6, one can clearly see that the lower tank-level fluctuation caused by the forward square wave disturbance during 80-th second and 95-th second can be suppressed within 6.6 seconds, when it is controlled by the RBF-ARX-RPC algorithm. However, the RBF-ARX-TRPC [30] and the PID-M require more than 13.1 seconds and 15 seconds, respectively. From Figure 7, one can see that, when the reverse square wave disturbance vanishes, the RBF-ARX-RPC algorithm can stabilize the output $H_2(t)$ on the expected output faster than that of the other algorithms. In general, it is clearly seen that the proposed RPC algorithm has best trajectory tracking and disturbance rejection performance.

One drawback of general RPC algorithms is their relatively large online computational burden, which may limit their applicability. The real-time computation times of the two RPC algorithms in the step response experiment whose control results are shown in Figure 6 are shown in Figure 8. The software environment of the control implementation is based on the Matlab 2017b on Windows 10-based PC (Intel Core i7-9700 16GB-RAM), and the two RPC algorithms are all written in M language. From Figure 8, one can see that the RBF-ARX-RPC costs more computation time than the RBF-ARX-TRPC. But, the maximum computation time (1.41 second) of the RBF-ARX-RPC is less than the sampling period (1.5 second) of the control system. Therefore, the proposed RPC strategy can complete all operations during the sampling period. In order to further reduce the computation time of the proposed RPC strategy, we will try to study the partially offline computing and partially online synthesis RPC strategy based on the SD-ARX model in the future research.

5. Conclusions

Based on the time-varying coefficient information of the SD-ARX model, three polytopic state-space models are designed to wrap the dynamics of a class of nonlinear systems. Based on the established state-space models, a two-stage scheduling RPC without using the system's steady state information is proposed. Considering that the state of the system may not reach to the boundary of the convex polytopic sets, which are constructed using only the parameter boundary information of the SD-ARX model, directly in only one step, in this paper, the parameter variation rate information of the model is considered to further compress the size of the convex polytopic sets. From the simulation results and comparison of the water tank system, one can see that the proposed RPC algorithm improved the trajectory tracking and disturbance rejection performance.

Data Availability

The data used to support the findings of this study are available from the corresponding author upon request.

Conflicts of Interest

The authors declare that they have no conflicts of interest.

Acknowledgments

This work was supported by the National Natural Science Foundation of China (61903049), the Education Department of Hunan Province, China (Projects Nos. 18C0781 and 17C0131), and the Natural Science Foundation of Hunan Province, China (Project No. 2018JJ3561).

References

[1] M. L. Darby and M. Nikolaou, "MPC: current practice and challenges," *Control Engineering Practice*, vol. 20, no. 4, pp. 328–342, 2012.

[2] M. Ławryńczuk, "Explicit nonlinear predictive control algorithms with neural approximation," *Neurocomputing*, vol. 129, pp. 570–584, 2014.

[3] D. Q. Mayne, "Model predictive control: recent developments and future promise," *Automatica*, vol. 50, no. 12, pp. 2967–2986, 2014.

[4] M. V. Kothare, V. Balakrishnan, and M. Morari, "Robust constrained model predictive control using linear matrix inequalities," *Automatica*, vol. 32, no. 10, pp. 1361–1379, 1996.

[5] Y. Lu and Y. Arkun, "Quasi-min-max MPC algorithms for LPV systems," *Automatica*, vol. 36, no. 4, pp. 527–540, 2000.

[6] Y. Lu and Y. Arkun, "A scheduling quasi-min-max model predictive control algorithm for nonlinear systems," *Journal of Process Control*, vol. 12, no. 5, pp. 589–604, 2002.

[7] D. Q. Mayne, M. M. Seron, and S. V. Raković, "Robust model predictive control of constrained linear systems with bounded disturbances," *Automatica*, vol. 41, no. 2, pp. 219–224, 2005.

[8] D.-F. He, H.-B. Ji, and L. Yu, "Constructive robust model predictive control for constrained non-linear systems with disturbances," *IET Control Theory & Applications*, vol. 7, no. 15, pp. 1869–1876, 2013.

[9] Z. Yan and J. Wang, "Robust model predictive control of nonlinear systems with unmodeled dynamics and bounded uncertainties based on neural networks," *IEEE Transactions on Neural Networks and Learning Systems*, vol. 25, no. 3, pp. 457–469, 2014.

[10] D.-F. He, H. Huang, and Q.-X. Chen, "Quasi-min-max MPC for constrained nonlinear systems with guaranteed input-to-state stability," *Journal of the Franklin Institute*, vol. 351, no. 6, pp. 3405–3423, 2014.

[11] B. Ding and H. Pan, "Dynamic output feedback-predictive control of a takagi-sugeno model with bounded disturbance," *IEEE Transactions on Fuzzy Systems*, vol. 25, no. 3, pp. 653–667, 2017.

[12] J.-H. Park, T.-H. Kim, and T. Sugie, "Output feedback model predictive control for LPV systems based on quasi-min-max algorithm," *Automatica*, vol. 47, no. 9, pp. 2052–2058, 2011.

[13] B. Ding, Y. Xi, M. T. Cychowski, and T. O'Mahony, "A synthesis approach for output feedback robust constrained model predictive control," *Automatica*, vol. 44, no. 1, pp. 258–264, 2008.

[14] D. Q. Mayne, S. V. Raković, R. Findeisen, and F. Allgöwer, "Robust output feedback model predictive control of constrained linear systems," *Automatica*, vol. 42, no. 7, pp. 1217–1222, 2006.

[15] B. Ding, "Constrained robust model predictive control via parameter-dependent dynamic output feedback," *Automatica*, vol. 46, no. 9, pp. 1517–1523, 2010.

[16] B. Ding, P. Wang, and J. Hu, "Dynamic output feedback robust MPC with one free control move for LPV model with bounded disturbance," *Asian Journal of Control*, vol. 20, no. 2, pp. 755–767, 2018.

[17] J. Du, X. Hu, H. Liu, and C. L. P. Chen, "Adaptive robust output feedback control for a marine dynamic positioning system based on a high-gain observer," *IEEE Transactions on Neural Networks and Learning Systems*, vol. 26, no. 11, pp. 2775–2786, 2015.

[18] B. Ding and T. Zou, "A synthesis approach for output feedback robust model predictive control based-on input-output model," *Journal of Process Control*, vol. 24, no. 3, pp. 60–72, 2014.

[19] H. S. Abbas, R. Toth, N. Meskin, J. Mohammadpour, and J. Hanema, "A robust MPC for input-output LPV models,"

IEEE Transactions on Automatic Control, vol. 61, no. 12, pp. 4183–4188, 2016.

[20] M. Gan, H.-X. Han-Xiong Li, and H. Hui Peng, "A variable projection approach for efficient estimation of RBF-ARX model," *IEEE Transactions on Cybernetics*, vol. 45, no. 3, pp. 462–471, 2015.

[21] H. Peng, T. Ozaki, V. Haggan-Ozaki, and Y. Toyoda, "A parameter optimization method for radial basis function type models," *IEEE Transactions on Neural Networks*, vol. 14, no. 2, pp. 432–438, 2003.

[22] X. Zeng, P. Hui, and Z. Feng, "A regularized SNPOM for stable parameter estimation of RBF-AR(X) model," *IEEE Transactions on Neural Networks and Learning Systems*, vol. 29, no. 4, pp. 779–791, 2017.

[23] P. J. Casanova-Peláez, F. Cruz-Peragón, J. M. Palomar-Carnicero, R. Dorado, and R. López-García, "RBF-ARX model of an industrial furnace for drying olive pomace," *Energy Conversion and Management*, vol. 64, pp. 106–112, 2012.

[24] F. Zhou, H. Peng, W. Ruan et al., "Cubic-RBF-ARX modeling and model-based optimal setting control in head and tail stages of cut tobacco drying process," *Neural Computing & Applications*, vol. 30, no. 4, pp. 1039–1053, 2016.

[25] H. Peng, K. Nakano, and H. Shioya, "Nonlinear predictive control using neural nets-based local linearization ARX model-stability and industrial application," *IEEE Transactions on Control Systems Technology*, vol. 15, no. 1, pp. 130–143, 2007.

[26] F. Zhou, H. Peng, Y. Qin, X. Zeng, W. Xie, and J. Wu, "RBF-ARX model-based MPC strategies with application to a water tank system," *Journal of Process Control*, vol. 34, pp. 97–116, 2015.

[27] J. Wu, H. Peng, K. Ohtsu, G. Kitagawa, and T. Itoh, "Ship's tracking control based on nonlinear time series model," *Applied Ocean Research*, vol. 36, pp. 1–11, 2012.

[28] H. Peng, G. Kitagawa, J. Wu, and K. Ohtsu, "Multivariable RBF-ARX model-based robust MPC approach and application to thermal power plant," *Applied Mathematical Modelling*, vol. 35, no. 7, pp. 3541–3551, 2011.

[29] F. Zhou, H. Peng, X. Zeng, X. Tian, and X. Peng, "RBF-ARX model-based robust MPC for nonlinear systems with unknown and bounded disturbance," *Journal of the Franklin Institute*, vol. 354, no. 18, pp. 8072–8093, 2017.

[30] F. Zhou, H. Peng, X. Zeng, and X. Tian, "RBF-ARX model-based two-stage scheduling RPC for dynamic systems with bounded disturbance," *Neural Computing and Applications*, vol. 31, no. 8, pp. 4185–4200, 2019.

[31] A. Casavola, D. Famularo, and G. Franzè, "A predictive control strategy for norm-bounded LPV discrete-time systems with bounded rates of parameter change," *International Journal of Robust & Nonlinear Control*, vol. 18, no. 7, pp. 714–740, 2008.

[32] M. Jungers, R. C. L. F. Oliveira, and P. L. D. Peres, "MPC for LPV systems with bounded parameter variations," *International Journal of Control*, vol. 84, no. 1, pp. 24–36, 2011.

[33] D. Li and Y. Xi, "The feedback robust MPC for LPV systems with bounded rates of parameter changes," *IEEE Transactions on Automatic Control*, vol. 55, no. 2, pp. 503–507, 2010.

[34] P. Zheng, D. Li, Y. Xi, and J. Zhang, "Improved model prediction and RMPC design for LPV systems with bounded parameter changes," *Automatica*, vol. 49, no. 12, pp. 3695–3699, 2013.

[35] F. A. Cuzzola, J. C. Geromel, and M. Morari, "An improved approach for constrained robust model predictive control," *Automatica*, vol. 38, no. 7, pp. 1183–1189, 2002.

[36] D. Angeli, A. Casavola, and E. Mosca, "Constrained predictive control of nonlinear plants via polytopic linear system embedding," *International Journal of Robust and Nonlinear Control*, vol. 10, no. 13, pp. 1091–1103, 2000.

[37] H. Pan, H. Wong, V. Kapila, and M. S. de Queiroz, "Experimental validation of a nonlinear backstepping liquid level controller for a state coupled two tank system," *Control Engineering Practice*, vol. 13, no. 1, pp. 27–40, 2005.